ARTICLE NO. 79-4106

Demonstration of Aircraft Wing/Store Flutter Suppression Systems

Chintsun Hwang,* Bertil A. Winther,† and George R. Mills‡
Northrop Corporation, Hawthorne, Calif.

Thomas E. Noll§
Air Force Flight Dynamics Laboratory, Wright-Patterson Air Force Base, Ohio
and
Moses G. Farmer§
NASA Langley Research Center, Hampton, Va.

A wind tunnel test program was conducted to demonstrate the active wing/store flutter suppression systems on a lightweight fighter aircraft. The program, completed in mid-1978, included the design, analysis, fabrication, and testing of a scale model. The tests were conducted at the NASA Langley 16-ft Transonic Dynamics Tunnel. Three store configurations were selected for testing. Two of these configurations were deliberately designed to exhibit low flutter speeds with rapid reductions in damping at the incipient flutter condition. After initial tunnel entries, which showed the need for certain improvements in the model and the control system design, substantial increases in the flutter speeds were achieved using both leading- and trailing-edge control surfaces, separately. For the most critical configuration, a demonstrated improvement of 18% and a projected improvement of 29% in the dynamic pressure were achieved.

Introduction

THE increase in strength of materials and the use of thin, low-drag airfoils have led to flexible and more flutter-prone wings. With many combinations of external stores, modern fighter aircraft have a wide variety of flutter placards that restrict operational use. In fact, an aircraft carrying external stores may have several flutter-speed restrictions on a single flight. In order to reduce the severity of these restrictions and take advantage of recent improvements in controls technology for high-performance aircraft, a logical approach is to develop a flutter suppression system that could eventually employ the same component used for conventional stability augmentation. Before a working flutter suppression system can be installed in an aircraft, a number of design aspects have to be considered. These aspects include selection of control surfaces and related actuation systems, definition of appropriate control laws applicable to a large variety of configurations and flight conditions, and development of redundancy and fail-safe features.

Automatic feedback systems controlling the aeroelastic response have been used successfully on several aircraft. The applications to date have been for augmentation of static stability, improvement of ride quality, reduction of maneuver loads, and suppression of structural loads induced by atmospheric turbulence. Considerable interest has emerged in recent years toward adding an active flutter-control function to the flight control systems. A pioneering investigation was conducted in 1968,[1] paving the way for a flight test program that employed a B-52 aircraft to demonstrate the feasibility of active flutter suppression. In Ref. 2, active flutter suppression tests were conducted on a wind-tunnel model of the B-52 to obtain comparisons with flight test data. Other efforts in the United States included a wind-tunnel test program[3] on an SST wing and an analytical study[4,5] of a wing/store flutter suppression system. Outside of the United States, considerable activity in the area of flutter suppression has been evidenced by several publications from England, France and Germany. Significant contributions in terms of wind-tunnel test demonstrations include Refs. 6 and 7. An interesting analytical study of active flutter suppression is presented in Ref. 8.

The work described in this paper is a demonstration program to resolve a number of technical problems and to prove the feasibility of flutter suppression systems for fighter aircraft with multiple stores. The program consisted of the model design and fabrication, the pre- and post-test analyses, and three wind tunnel entries conducted at the NASA Langley Transonic Dynamics Tunnel.

Description of the Model

The test specimen is a 30% scale, semispan (right half) model of a lightweight fighter aircraft. The configuration is characterized by a moderately swept wing with a large, highly swept leading edge extension (LEX) at the root, differential area ruling of the fuselage and underwing engine inlets with slots for fuselage boundary-layer diversion. The model was designed such that, for three selected store configurations, the unaugmented flutter speeds plus the desired improvements with the AFSS (Active Flutter Suppression Systems) operative, could be demonstrated within the test limits of the NASA Langley 16-ft Transonic Dynamics Tunnel (TDT). Pertinent scale factors based on freon as the flow medium are presented in Table 1.

The model simulates all important wing, pylon, rigid body, and fuselage degrees of freedom that are required to provide correct modal coupling for flutter. A schematic drawing is shown in Fig. 1. The wing has an aluminum spar with

Received May 22, 1978; revision received Jan. 23, 1979.

Index categories: Structural Dynamics; Testing, Flight and Ground; Aeroelasticity.

*Manager, Structural Dynamics Research Dept. Associate Fellow AIAA.
†Engineering Specialist. Member AIAA.
‡Sr. Technical Specialist.
§Aerospace Engineer. Member AIAA.

Table 1 Model scale factors

Dimension	Symbol	Scale
Length	L	0.300
Time	T	0.665
Velocity	L/T	0.451
Frequency	$1/T$	1.503
Dynamic pressure	M/LT^2	0.127
Mass	M	0.0169
Force	ML/T^2	0.0115
Flexibility	T^2/M	26.18

segmented balsawood covering. The half fuselage is simulated by a segmented metal shell attached to a magnesium beam which is restrained in its lateral degrees of freedom by three bar mechanisms mounted on the tunnel wall. In addition, the model is supported by a lift cable and by two preloaded (450N) fuselage cables running around pulleys so that the model is free to move in plunge and pitch and, to a lesser degree, in the axial direction. To obtain smooth flow past the fuselage, a splitter plate is installed close to the symmetry plane. The model is trimmed by an all-movable and remotely controlled horizontal tail. A narrow-span leading-edge flap and a trailing-edge surface were selected as the active flutter suppression devices. They are actuated by miniature hydraulic actuators. Accelerometers are installed inside the wing to sense the vibration. After proper conditioning, the signals are fed to the servo-valve which supplies hydraulic pulses to the actuator. A potentiometer is installed in the hinge mechanism to sense the control-surface rotation and provide input to the actuator servo.

Analytical Study

Initial Flutter Analysis

Several flutter analyses were made to determine the most interesting configurations for the test program. Trend studies were performed with variations of store mass, center of gravity, moment of inertia, pylon attachment, etc. Linearized finite elements models of the aeroelastic system were employed in the conventional manner, with the dynamic equation formulated in terms of generalized coordinates including a representative number of natural vibration modes and appropriate rigid body modes. Unsteady aerodynamic loadings were computed by use of the doublet-lattice method at three discrete Mach numbers in the subsonic regime. Three external store configurations that differ substantially in their flutter characteristics were selected for further analysis and wind-tunnel testing. The configurations are the following:

configuration A: Tip launcher rail: AIM-9E (Sidewinder)
Tip pylon (95% span): Not installed
Inboard pylon (65% span): AIM-7 Sparrow (3 in. aft)

configuration B: Tip launcher rail: Empty
Tip pylon: AIM-7 (3 in. aft)
Inboard pylon: Not installed

configuration C: Tip launcher rail: Empty
Tip pylon: AIM-9E (6 in. aft)
Inboard plylon: Not installed

Figure 2 presents analytical results for the three selected configurations. The preliminary flutter analysis of configuration A predicted a "hump" mode at about 13 Hz in model scale with a slow decrease in damping as the flutter speed is approached. As shown in Fig. 2, this characteristic results in an unusual increase of the flutter dynamic pressure at Mach numbers approaching unity. Configuration B exhibits a conventional bending-torsion type of flutter at around 7 Hz with a violent onset. It should be noted that this flutter condition was created by attaching a wing pylon in the tip region with the store located in an extreme aft position. Similarly, a violent type of flutter was predicted for configuration C, at the higher frequency, 10.5 Hz, due to the reduced store mass.

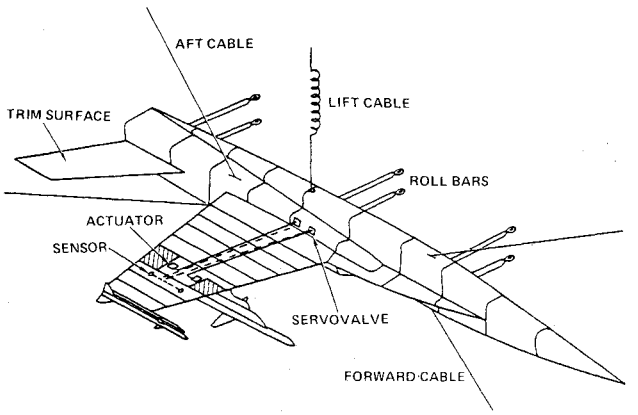

Fig. 1 Wing/store model with active flutter control, configuration A.

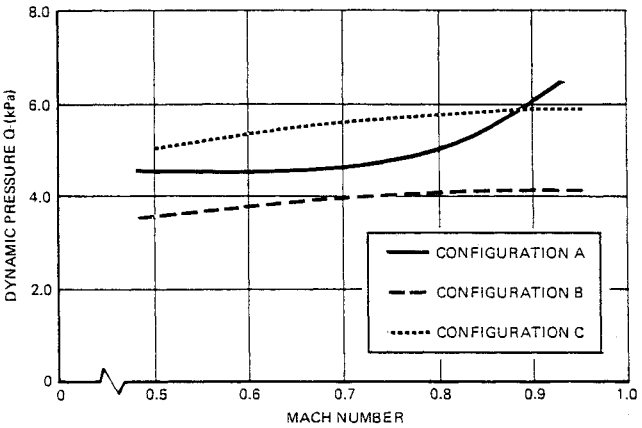

Fig. 2 Model flutter boundaries.

Design Analysis

Design analyses of the active flutter suppression systems for each configuration were performed to establish control laws, compressibility effects, transducer and control surface locations, etc. For this purpose new analytic techniques were developed to cope with the frequency-dependence of the control system terms, which render the conventional eigenvalue solution techniques impractical. One satisfactory solution method used in the program is the Characteristic Diagram technique suggested by Landahl[9] and developed at Northrop[10] into an operational program. The method involves plotting of the characteristic equation in the complex plane at a given speed/altitude combination with the frequency as the parameter. Input frequency is specified by a subroutine that computes an automatic frequency sweep. The sweep rate is reduced as a root is approached, thus defining the characteristic diagram with sufficient accuracy. The damping of the dynamic system is determined directly from the shape of the diagram.

Another analysis technique is the Transfer Function Synthesis (TFS) technique,[11] which has proven to be both practical and accurate for most of the present design analyses. The TFS technique is a computerized procedure for obtaining closed-form approximations to aeroelastic transfer functions, including the effects of inertial, elastic and aerodynamic forces. The transfer functions are synthesized from analytical

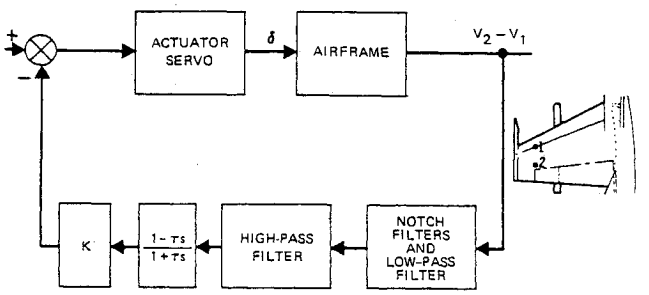

Fig. 3 Block diagram of the flutter suppression loop.

frequency-response data as ratios of polynomials in terms of the Laplace variable S. When designing a flutter suppression system based on the transfer function data, it was found important to maximize the relative response in the flutter mode so that the active system at nominal gain values performs without undue excitation of the adjacent modes.

The block diagram presented in Fig. 3 illustrates the flutter suppression system used in the test program. In order to insure the stability of the adjacent modes, several filters are used to condition the feedback signal $(V_2 - V_1)$, which is the differential voltage delivered by two accelerometers located at 70% of the wing span. A differential acceleration of one g (9.8 m/s^2) provides a voltage of approximately 0.2 V. Two notch filters at 90 Hz and 34 Hz were required to eliminate ground resonances in the structural panels adjoining the actuator. A second-order low-pass filter (breaking at 42 Hz) was found to eliminate resonance in high-order vibration modes such as the tip missile bending mode. The purpose of the high-pass filter is to minimize the coupling between the structural vibration modes and the rigid-body modes introduced by the suspension system. In the present program, emphasis was placed on simplicity in design and fabrication of the flutter suppression system. To satisfy this requirement, it was found that the most desirable filter for compensation of the flutter mode is a first-order variable gain/phase network as shown in the block diagram. A dial on the control panel is used to adjust the gain values in the range 0.0-2.0. Similarly, using another dial, the time constant τ of the phase compensation can assume values between 0.0 and 0.05 s.

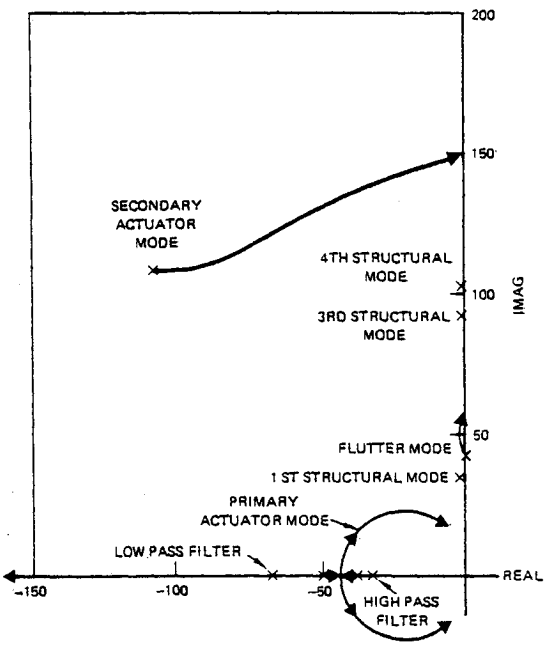

Fig. 4 Root locus of configuration B leading-edge control, $M = 0.0$, $V = 370.4$ km/h.

Extensive analyses were performed to determine the optimal gain/phase settings for various dynamic pressures and Mach numbers. The approximations of the aeroelastic response at various speeds and Mach numbers were used to obtain root locus plots with the loop gain as the parameter. Figure 4 presents a typical root locus plot for configuration B with leading-edge control, at a speed slightly exceeding the flutter speed. It is observed that all poles associated with structural vibration modes are located close to the imaginary axis. Another finding is that the flutter suppression system has an adverse effect on the first wing-bending mode, which becomes unstable at high loop gains. Due to this limiting factor on the allowable loop gain, the flutter suppression system is able to stabilize the system only up to moderate dynamic pressures, as demonstrated in Figs. 5 and 6 which present magnified views of the roots associated with the first two structural modes. All roots associated with the actuator servo and the filters are sufficiently stable for normal gain values.

Similar analyses were performed for the other configurations with both leading- and trailing-edge controls, at various Mach numbers. The trailing-edge system for configuration A was found to be very effective in suppressing the "hump" mode flutter. For configuration C, as for B, the analysis predicted that the leading-edge surface would be more effective in controlling the flutter mode. For both configurations, however, the allowable gain was limited by the destabilizing effect predicted for the root associated with fundamental wing bending.

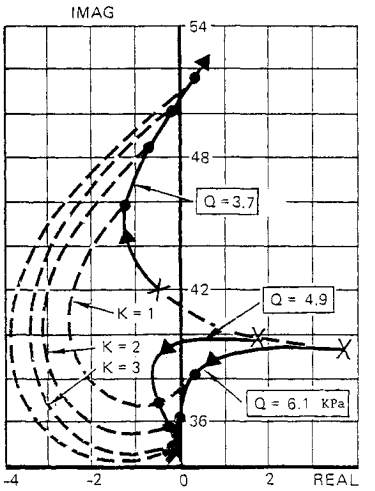

Fig. 5 Flutter mode root locus, configuration B, leading-edge control, $M = 0.8$.

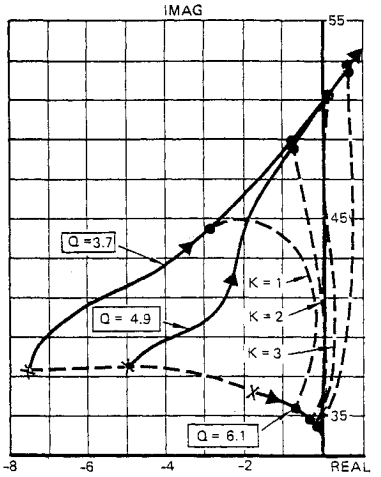

Fig. 6 First bending mode root locus, configuration B, leading-edge control, $M = 0.8$.

Ground Vibration Test

The initial ground vibration test (GVT) was conducted in April 1977. Two different types of vibration tests were performed. The conventional type utilized discrete, sinusoidal shaker input at each natural frequency. Relative accelerations were measured by a roving accelerometer. Due to the time-consuming nature of this test, it was completed for configuration A only. The second type of GVT utilized a Hewlett-Packard Fourier Analyzer, System 5451B. The wind-tunnel model was excited by random noise input to a shaker located in the fuselage nose. The response was measured consecutively at preselected stations and transmitted to the computer. Almost simultaneously with the data transmittal, the transfer function for each test point was computed and stored on disk. Sampling time per point was approximately 120 s, and the frequency resolution was 0.2 Hz. The transfer function data stored on disk were used to determine the modal deflections at approximately 85 points for each of the three configurations. To extract accurate measurements of the modal damping, a zoom technique was employed with data sampled at a few locations during approximately 600 s. Figure 7 presents a typical transfer function computed by the Fourier Analyzer. Even though all modes generated by the Fourier Analyzer between 0 and 50 Hz are clearly identifiable, the shapes of the low-frequency modes show poor correlation with the corresponding modes measured in the conventional GVT or the ones obtained from analysis. The results for higher-order modes are satisfactory. Later, during each wind-tunnel entry, the conventional vibration test was repeated to verify the structural integrity of the model and determine the influence of the suspension system.

Functional checks of the actuator servos and other components in the control system were made both in a bench test and with the system installed in the model. Open-loop tests were performed to measure the servo output versus input command. The gains of the actuation loop were set for optimum closed-loop response, which then was modified by various filters to match a typical aileron actuator. After completion of the functional tests, the flutter suppression loop was closed to determine the loop gain at ground resonance. Due to the potential danger to the model, precautions were taken to limit the hydraulic flow rate provided by the servo-valve. Notch filters were inserted in the flutter suppression loop to eliminate critical modes. To further increase the available loop gain, the notch filters were modified and a second-order low-pass filter inserted during the second wind tunnel entry.

From the input and output signals of the actuator servo, a transfer function as shown in Fig. 8 was derived and compared to the discrete data measured in the functional test. The low-frequency response of the actuator servo is referenced to 3.8 deg/V. After the first wind-tunnel entry, the servo was completely redesigned and the frequency response was modified to some extent in the high-frequency band.

Wind-Tunnel Tests

First Entry

The wind-tunnel test program was conducted in three separate entries during June, August and December 1977. In the first entry, the leading-edge surface was used for sweep-excitation of configuration A. A rapidly diverging oscillation of the leading-edge servo was encountered well below the predicted flutter speed.

In reviewing the test results from the first entry, a decision was made to redesign the actuator servos. A detailed analysis of the leading-edge servo was performed considering the destabilizing effect of the air loads. Figure 9 demonstrates that the root associated with an integrator in the forward servo-loop couples with the root associated with the airload on the leading-edge control. With maximum attainable loop gain, the analysis shows that the system was only marginally stable. Based on this analysis, the first step was to eliminate the integrator and redesign the servo. At the same time, a number of precautionary measures were undertaken to increase the dynamic stiffness of the servos. The pressure feedback used in combination with position feedback in the servo loop was eliminated and the hydraulic supply pressure was doubled to 13,800 kPa.

Second Entry

In the second wind-tunnel entry, the flutter boundary of configuration A was explored. The analysis of this configuration had predicted a moderately unstable "hump" mode with significant participation of the fuselage first bending mode. Unexpectedly high damping in the model support system, however, changed the dynamic coupling and made the predicted flutter mode stable. Nevertheless, the test demonstrated that the control system increased the damping and decoupled the modes participating in the expected flutter mechanism.

During testing of configuration B, sweep excitation using the trailing-edge control surface was performed to measure damping levels and define the flutter boundary with the flutter suppression system inactive. For Mach number 0.8, a violent wing torsional oscillation was encountered at a dynamic pressure of 3.64 kPa when the trailing-edge control surface was used in a frequency sweep to excite the model. The model experienced some damage and the test was terminated for repair.

Third Entry

The third tunnel entry was initiated with testing of a modified configuration A having a mass of 0.2 kg added to the AIM-9E missile tip. During this test, most damping trends

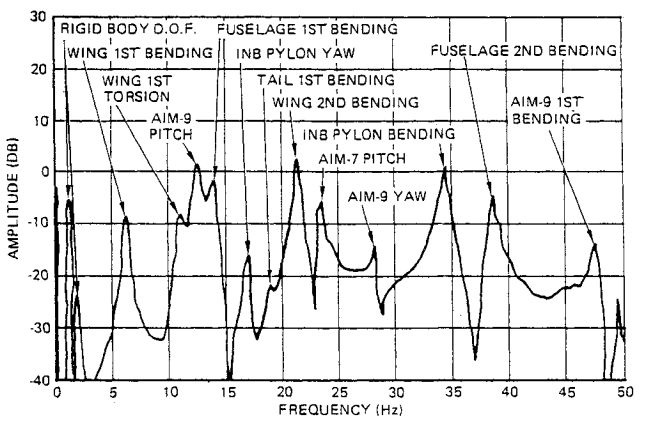

Fig. 7 Acceleration at leading-edge pickup due to random input at fuselage nose, configuration A.

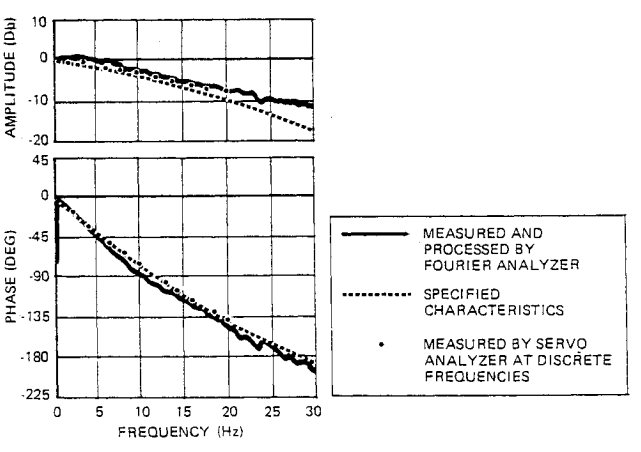

Fig. 8 Transfer function of trailing-edge servo.

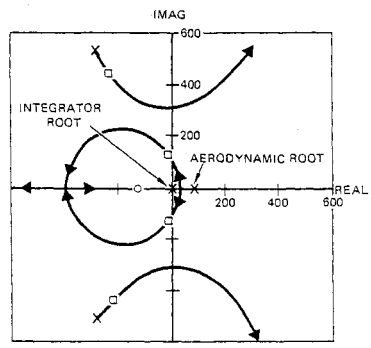

Fig. 9 Root locus of leading-edge servo in first tunnel entry.

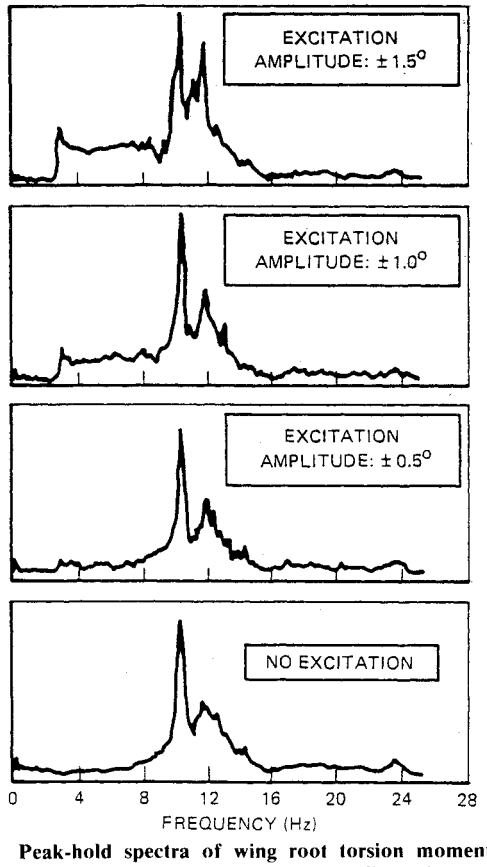

Fig. 10 Peak-hold spectra of wing root torsion moment due to leading-edge control sweep and turbulence, configuration A, $M=0.9$, $Q=5.75$ kPa.

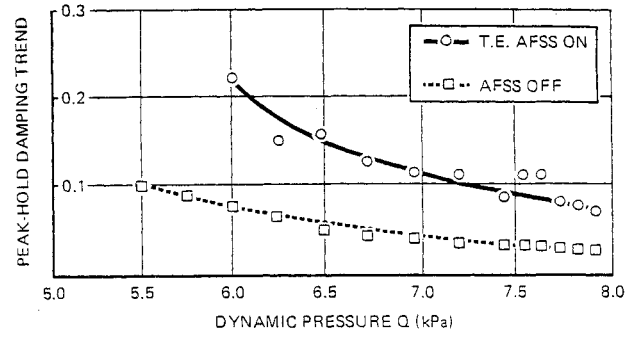

Fig. 11 Damping trend, trailing-edge system, configuration A, $M=0.8$.

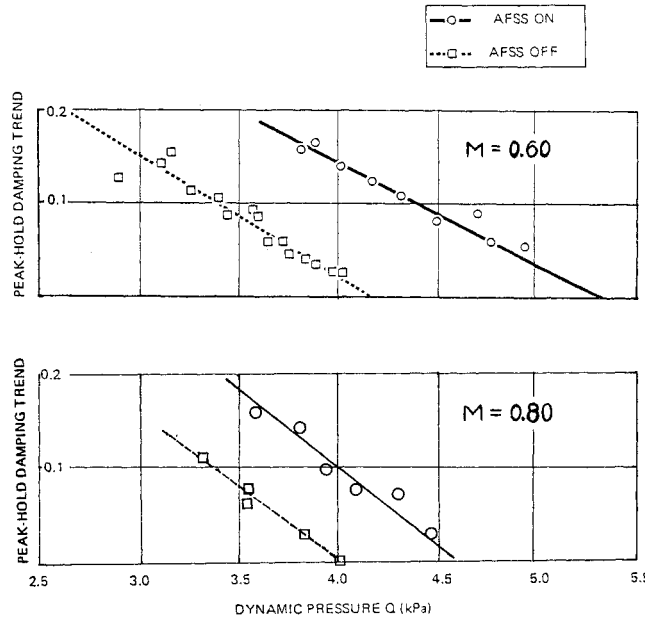

Fig. 12 Damping trend for configuration B, leading-edge system.

were obtained using the peak-hold spectrum method, which provides Fourier-transformed measurements of the response, filtered through 250 narrow-band circuits. The peak response within each interval is registered on a screen, permitting the test engineer to determine when the resulting spectrum has converged and the data sampling can be discontinued. The damping of a resonating mode is proportional to the inverse of the peak-hold amplitude. Figure 10 illustrates the model response in terms of peak-hold spectra of the wing root torsion moment due to either tunnel turbulence alone or tunnel turbulence in combination with sweep excitation by the leading-edge control surface. Figure 11 presents a peak-hold damping trend for configuration A with and without flutter suppression. As in the previous tunnel entry, it was demonstrated that the trailing-edge control system provided a significant amount of damping, but friction in the model suspension system was sufficient to prevent flutter for this configuration.

The test continued with configurations B and C, which were designed specifically to have severe flutter onset. Figure 12 presents measured damping trends for configuration B at Mach numbers 0.6 and 0.8. The model sustained slight damage at $M=0.8$ where a "hard" flutter point was obtained. Subsequently, considerable increases in the flutter speeds were achieved using the leading-edge control surface. For configuration B at Mach number 0.6, a demonstrated improvement of 18% and a projected improvement of 29% in the dynamic pressure were achieved. As predicted by analysis, the increased damping in the flutter mode was traded for a destabilizing effect on the first wing-bending mode. For this reason, the nominal loop gain in the flutter suppression system was limited to 0.7. The frequency shifts predicted by the analysis for system-on were also substantiated by the test showing a sudden drop in the torsion frequency as the dynamic pressure approached its critical value. The damping data of Fig. 13 were confirmed, allowing reasonable deviations, by post-test analysis of analog tape records using a moving-block/randomdec technique as described in Ref. 12.

Similar test results were obtained for configuration C. As for configuration B, the critical mode with the flutter suppression system on was the first wing-bending mode. The effect of the leading-edge system on the peak-hold response is presented in Fig. 13. Since in this case the projected dynamic pressure at flutter was 5.10 kPa, the upper two plots demonstrate the effectiveness of the closed-loop system. Similar data were obtained with the trailing-edge system in operation. Damping trends at Mach 0.6 are presented in Fig. 14 with the leading- and trailing-edge systems.

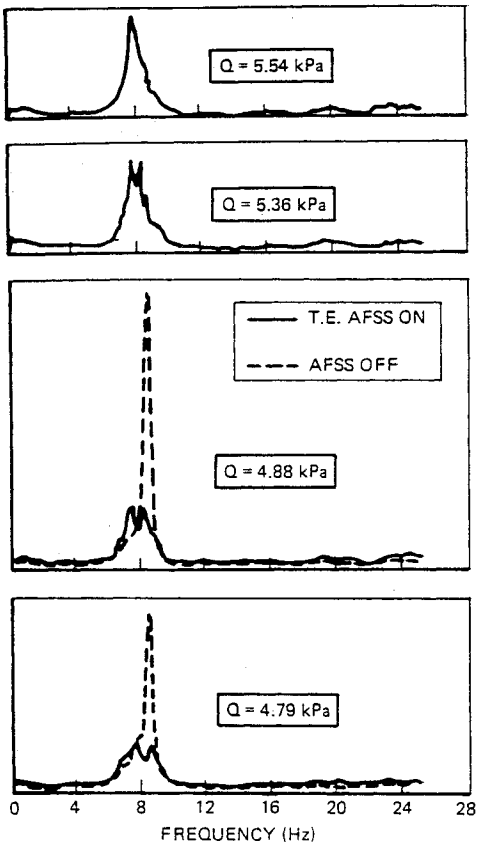

Fig. 13 Peak-hold spectra of wing root torsion moment for configuration C with leading-edge control, $M=0.6$. Projected flutter dynamic pressure $Q=5.10$ kPa.

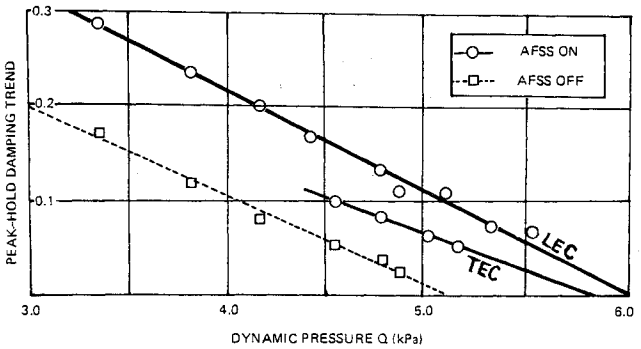

Fig. 14 Damping trends for configuration C, $M=0.6$, using either leading-edge control (LEC) or trailing-edge control (TEC).

Analytical Correlation with Test Data

Analysis without AFSS

Additional flutter analyses were conducted for each of the unaugmented configurations using the FOP module of the FASTOP (Flutter and Strength Optimization Program) computer program.[13] For configuration A at $M=0.8$, flutter was predicted at a dynamic pressure of 6.69 kPa using computed vibration modes and at a dynamic pressure of 6.56 kPa using ground vibration test data. It was noted earlier that this configuration would not flutter in the tunnel due to unexpectedly high damping in the support system. For configuration B, the corresponding numbers were 3.64 kPa and 4.11 kPa. Using computed modes, the analysis was about 10% conservative. With measured modes it was about 2% unconservative. The analysis for configuration C at $M=0.6$ using computed vibration modes, predicted a flutter instability at 4.93 kPa, 2% below the projected test point.

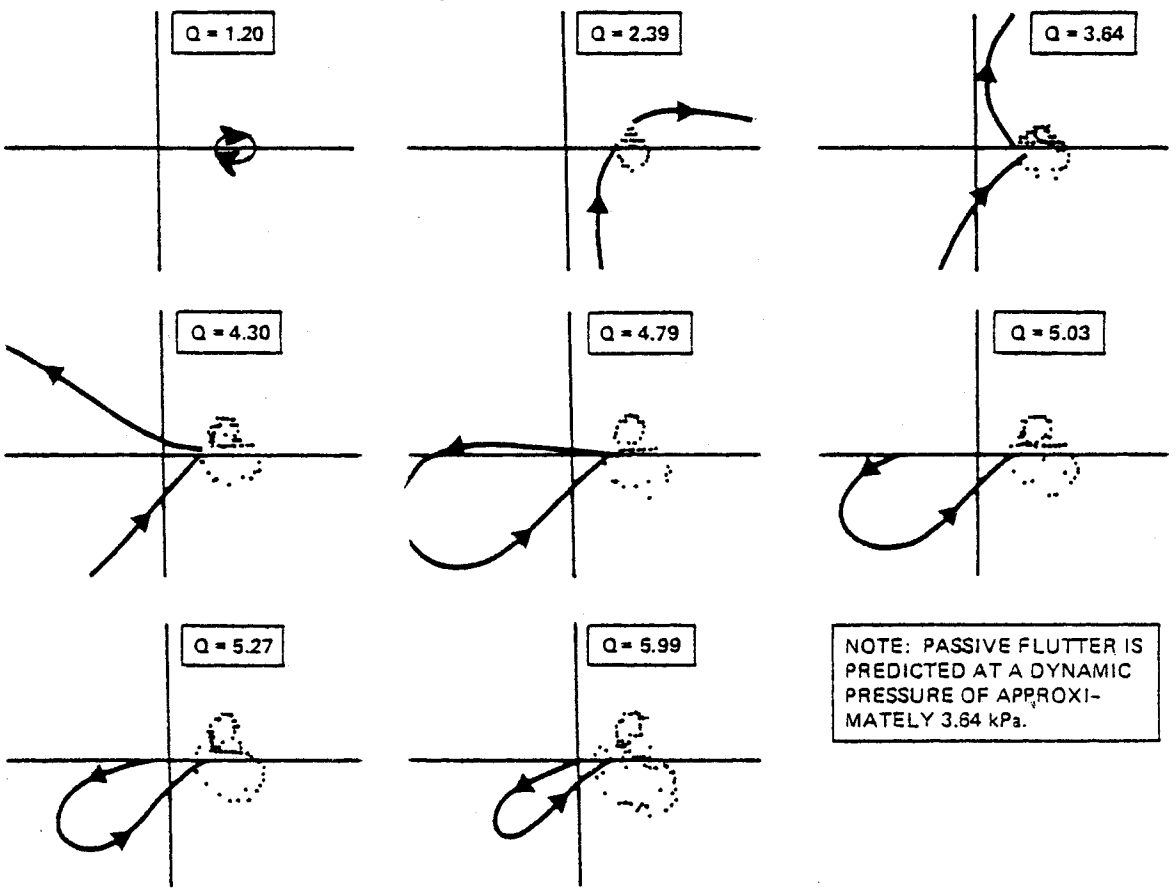

Fig. 15 Modified Nyquist plots for configuration B, leading-edge system, $M=0.8$.

Analysis with AFSS

To determine the stability characteristics of the augmented model, a frequency domain procedure with a modified Nyquist criterion was employed. Figure 15 presents a series of Nyquist plots for configuration B with leading-edge control at $M=0.8$. At low dynamic pressure, where the response is small, the loop corresponding to the critical mode is small and located to the right of the origin. As the flutter speed is approached, the Nyquist loop gets larger and approaches a curve of infinite radius that turns in the clockwise direction. At flutter, the loop degenerates to a straight line. As the flutter speed is surpassed, the critical mode encircles the origin in a counterclockwise manner indicating that the model is stable. For higher speeds (above flutter), the Nyquist loop becomes smaller until it no longer encircles the origin. At this point, suppression of the flutter mode is lost. For configuration B, $M=0.8$, loss of flutter control was predicted at a dynamic pressure of 5.27 kPa. This represents an increase of 31% in flutter dynamic pressure over the unaugmented test case. Experimental results at this Mach number indicated a projected increase of 16% using the peak-hold trend and a projected increase of 23% using the estimated damping ratios.

The analyses for the augmented configuration A at $M=0.8$ showed that the critical dynamic pressure could be increased by about 40% using either the leading-edge or the trailing-edge surface. Since this configuration was stable in the tunnel, it is difficult to make a meaningful comparison. For the augmented configuration C with leading-edge control, the analysis at $M=0.6$ showed good stability characteristics up to a dynamic pressure of 7.79 kPa, which is 55% above the unaugmented case. The test results, however, show a projected improvement of only 18%.

In general, control-surface aerodynamic force and moment coefficients predicted by theory are high when compared to experimental data. Since experimental information on this model regarding control surface aerodynamics was not available, there was no attempt at this time to reduce the magnitude of the control-surface aerodynamics. Unmodified control surface aerodynamics tend to predict a more efficient active flutter suppression system. This may be a partial explanation of the differences obtained between the analysis and test results.

Concluding Remarks

Although many problems remain to be solved in order to make a flutter control system truly acceptable as routine equipment, the present test program has demonstrated that active suppression of wing/store flutter is feasible for practical application. As far as was known, this was the first time that a leading-edge surface was used as the single active device for flutter control. Both the leading- and the trailing-edge surfaces were used independently to suppress a single flutter mode.

Future flutter suppression systems would most likely be tied to special-purpose computers responding in an adaptive manner to counteract the structural response. For instance, presently-available computers with a built-in algorithm to efficiently identify the basic modal data may be applied to synthesize control laws. Even more powerful computer equipment may be needed to handle flutter suppression on a real time basis.

Acknowledgments

The work presented in this paper was carried out at Northrop Corporation under AFFDL Contract F33615-76-C-3039, in cooperation with NASA Langley Research Center.

References

[1]Morris, P.M. and Bender, M.A., "Aircraft Load Alleviation and Mode Stabilization (LAMS)," AFFDL-TR-68-158, Dec. 1968.

[2]Sevart, D.F., "Development of Active Flutter Suppression Wind-Tunnel Testing Technology," AFFDL-TR-74-126, Jan. 1975.

[3]Sanford, M.C., Abel, I., and Gray, D.L., "Development and Demonstration of a Flutter-Suppression System Using Active Controls," NASA TR R-450, Dec. 1975.

[4]Triplett, W.E., Kappus, H.P.F., and Landy, R.J., "Active Flutter Suppression Systems for Military Aircraft—A Feasibility Study," AFFDL-TR-72-116, Feb. 1973.

[5]Triplett, W.E., Landy, R.J., and Irwin, D.W., "Preliminary Design of Active Wing/Store Flutter Suppression Systems for Military Aircraft," AFFDL-TR-74-67, Aug. 1974

[6]Sensburg, O., Hönlinger, H., and Kuhn, M., "Active Control of Empennage Flutter," AGARD-CP-175, April 1975.

[7]Destuynder, R., "Essai En Soufflerie D'un Suppresseur De Flottement Sur Une Aile Droite," AGARD-CP-175, April 1975.

[8]Turner, M.R., "Active Flutter Suppression," AGARD-CP-175, April 1975.

[9]Landahl, M.T., "Graphical Technique for Analyzing Marginally Stable Dynamic Systems," *Journal of Aircraft,* Vol. 1, Sept.-Oct. 1964, pp. 293-299.

[10]Winther, B.A., "A Study on a Flutter Suppression System for the Northrop YF-17," Northrop Report NOR 74-64, July 1974.

[11]Arthurs, T.D., Tye, R.R., and Winther, B.A., "Aeroelastic Airframe Transfer Function Synthesis," *Proceedings of the AIAA/ASME/SAE 17th Structural Dynamics and Materials Conference,*, May 1976, pp. 383-388.

[12]Hammond, C.E. and Doggett, R.V., Jr., "Determination of Subcritical Damping by Moving-Block/Randomdec Applications," presented at the NASA Symposium on Flutter Testing Techniques, Oct. 1975.

[13]Wilkinson, K., Markowitz, J., Lerner, E., Chipman, R., and George, D., "An Automated Procedure for Flutter and Strength Analysis and Optimization of Aerospace Vehicles," AFFDL-TR-75-137, Vol. I and II, Dec. 1975.